

1 Testing the potential of using fine quartz for dating loess in South Island, New  
2 Zealand

3 A. Avram<sup>1,2</sup>, Z. Kabacińska<sup>2</sup>, A. Micallef<sup>3,4</sup>, A. Timar-Gabor<sup>1,2,\*</sup>

4 <sup>1</sup>*Faculty of Environmental Science and Engineering, Babes-Bolyai University, Cluj-Napoca, Romania*

5 <sup>2</sup>*Interdisciplinary Research Institute on Bio-Nano-Sciences, Environmental Radioactivity and Nuclear Dating Centre, Babes-Bolyai  
6 University, Cluj-Napoca, Romania*

7 <sup>3</sup>*Helmholtz Centre for Ocean Research, GEOMAR, Kiel, Germany*

8 <sup>4</sup>*Marine Geology & Seafloor Surveying, Department of Geosciences, University of Malta, Malta*

9 \* *Corresponding author:*

10 *A. Timar-Gabor: alida.timar@ubbcluj.ro*

11  
12 Abstract

13 The applicability of optically stimulated luminescence (OSL) dating on quartz from  
14 South Island, New Zealand is hampered by the poor behaviour of the targeted  
15 signals. However, most OSL dating studies have been focused on using coarse  
16 quartz fractions. Since a previous study conducted from a nearby site demonstrated  
17 that coarse quartz (63-90, 90-125, 125-180 and 180-250  $\mu\text{m}$ ) is not suitable for OSL  
18 dating, we attempt using fine quartz here. Therefore, the standard SAR protocol and  
19 two elevated temperature post-infrared infrared protocols (pIRIR<sub>225</sub> and pIRIR<sub>290</sub>)  
20 were applied on 4-11  $\mu\text{m}$  quartz and polymineral grains extracted from a  
21 loess/paleosol section. Unlike the coarser fractions, the OSL signal of fine quartz  
22 displayed satisfactory characteristics which allowed estimating ages ranging from  
23 0.3±0.04 ka to 16±1 ka. On the other hand, pIRIR ages overestimate quartz ages by 19  
24 to 122 % in the case of the application of the pIRIR<sub>225</sub> protocol and by 25 to 217% in  
25 the case of the application of the pIRIR<sub>290</sub> protocol. While in the case of the pIRIR<sub>290</sub>  
26 protocol, the overestimation can be partially attributed to unsatisfactory behaviour  
27 in terms of dose recovery tests, the age differences between fine quartz and  
28 polymineral fine grains pIRIR<sub>225</sub> are not fully explained. In order to understand the  
29 differences between the two quartz fractions, we characterise fine (4-11 $\mu\text{m}$ ) as well  
30 as the usually used coarser grain sizes (> 63  $\mu\text{m}$ ) of quartz by electron spin resonance

31 (ESR). No significant differences are reported in qualitative terms between the grain  
32 sizes investigated and calibration quartz. We report a higher abundance of intrinsic  
33 defects in the fine grain fraction; however, this is typical for quartz from other  
34 regions as well, that was amendable for OSL dating.

## 35 **1. Introduction**

36 Loess deposits of New Zealand are considered important archives for paleoclimate  
37 reconstruction of the southern hemisphere (Alloway et al., 2007), thus recent studies  
38 have been centred in establishing high-resolution chronologies.

39 Optically Stimulated Luminescence Dating (OSL) represents one of the most used  
40 dating techniques for Quaternary climate reconstruction. Its applicability has been  
41 successful for loess deposits located over both northern and southern hemispheres,  
42 respectively (Roberts 2008, 2015). However, since luminescence dating has been  
43 perceived to be challenging for loess sediments from South Island of New Zealand,  
44 few OSL studies have been reported so far (e.g., Holdaway et al., 2002; Rowan et al.,  
45 2012; Sohbati et al., 2016; Micallef et al., 2021; Brezeanu et al., 2021). Even though  
46 quartz is considered the preferred dosimeter when young sediments have to be  
47 dated due to the higher bleachability of the signal, it is well known that South Island  
48 quartz suffers from major problems that restrain its application, namely the weak  
49 sensitivity of the signal, with the signal originating from many dim grains and the  
50 poor behaviour exhibited in the single aliquot regenerative dose (SAR) protocol  
51 (Preusseur et al., 2006). These issues have been attributed by the aforementioned  
52 study to the short sedimentation history of the mineral grains, as it was reported that  
53 quartz sensitisation can be achieved by repeated irradiation/bleaching cycles. A  
54 recent study by Brezeanu et al. (2021) confirmed that the OSL signals of coarse (>63  
55  $\mu\text{m}$ ) quartz displayed low-sensitivity and a significant sensitivity-changes during  
56 the repeated SAR cycles. Despite these limitations, there are few OSL studies that  
57 reported ages on quartz in New Zealand (e.g., Holdaway et al., 2002; Nichol et al.,  
58 2003; Rowan et al., 2012; Hornblow et al., 2014; Sohbati et al., 2016). Holdaway et

59 **al., 2002** reported luminescence ages on 90-125  $\mu\text{m}$  quartz that were in agreement  
60 with  $^{14}\text{C}$  ages for colluvial sediments from Otago, South Island of New Zealand.  
61 Later, **Rowan et al., 2012** have successfully obtained a luminescence chronology for  
62 glaciofluvial sediments from Canterbury Plains of South Island using 180-211  $\mu\text{m}$   
63 quartz. Moreover, a more recent study conducted by **Sohbati et al., 2016** reported a  
64 good agreement between 40-63  $\mu\text{m}$  quartz SAR-OSL and pIRIR<sub>290</sub> luminescence ages  
65 in the attempt to refine palaeorockfall chronologies in New Zealand using  
66 luminescence dating.

67 Since the applicability of luminescence dating on quartz grains extracted from New  
68 Zealand sediments is not always a viable solution, other luminescence studies  
69 conducted on South Island considered that using infrared stimulated luminescence  
70 (IRSL) signal on coarse K-rich feldspars (**Preusseur et al., 2005**) or on polymineral  
71 fine grains (e.g., **Berger et al., 2001, 2002; Hormes et al., 2003; Rother et al., 2009;**  
72 **Almond et al., 2001, 2007; Schulmeister et al., 2010**) is a more appropriate solution  
73 for obtaining luminescence chronologies. It is well known that IRSL signal of  
74 feldspars suffers from anomalous fading and thus recent studies have developed  
75 measurements protocols that are able to circumvent fading. Such protocols consist of  
76 a double IR stimulation and they are known as post infrared-infrared stimulated  
77 luminescence protocols, pIRIR<sub>225</sub> and pIRIR<sub>290</sub>. Even though, these pIRIR protocols  
78 have been successfully applied on coarse K-feldspars as well as on polymineral fine  
79 grains extracted from loess deposits all over the world (e.g., **Roberts 2008; Buylaert**  
80 **et al., 2009, 2011; Thiel et al., 2011; Vasiliniuc et al., 2012; Yi et al., 2016; Bösken et**  
81 **al., 2017; Zhang et al., 2018; Veres et al., 2018; Avram et al., 2020; Avram et al.,**  
82 **2022**), their potential has not been fully explored on New Zealand sediments. Only  
83 three dating studies have reported pIRIR<sub>290</sub> luminescence ages (**Sohbati et al., 2016;**  
84 **Micallef et al., 2021; Brezeanu et al., 2021**) and two studies presented pIRIR<sub>225</sub>  
85 (**Micallef et al., 2021; Brezeanu et al., 2021**) chronologies on loess extracted from  
86 South Island of New Zealand.

1 87 To our knowledge, all quartz luminescence ages reported so far in literature were  
2 88 determined using coarse grains quartz (>63  $\mu\text{m}$ ), in this study we attempt for the  
3  
4 89 first time to apply SAR-OSL protocol on fine (4-11  $\mu\text{m}$ ) quartz extracted from loess in  
5  
6 90 the Canterbury Plains of South Island, New Zealand. In order to validate the quartz  
7  
8 91 ages, pIRIR<sub>225</sub> as well as pIRIR<sub>290</sub> protocols have been applied on polymineral fine  
9  
10 92 grains extracted from the same samples.

## 13 93 **2. Site description**

16 94 The foothills of the Southern Alps as well as the lowlands of the Canterbury Plains  
17  
18 95 represent the regions with the widest distribution of loess deposits in South Island of  
19  
20 96 New Zealand (Yates et al., 2018).

23 97 The investigated site (44.014973 °S, 171.891569 °E) is located on the southern part of  
24  
25 98 the Canterbury Plains and the eastern side of the South Island of New Zealand  
26  
27 99 (Figure S1). Three modern rivers namely Rakaia, Rangitata and Ashburton flow  
28  
29 100 perpendicularly to the eastern coastal cliff in the Canterbury Plains, discharging into  
30  
31 101 the Pacific Ocean. The loess section is situated nearby the site investigated by  
32  
33 102 Brezeanu et al. (2021) and therefore a more detailed description of the area can be  
34  
35 103 found in their study.

39 104 Luminescence investigations have been performed on seven samples collected at a  
40  
41 105 resolution of 20 cm. The uppermost sample, NZ 6 was collected from a depth of 10  
42  
43 106 cm while the last sample NZ 12 was collected at a depth of 130 cm.

46 107 ESR analysis presented in this study have been performed on sample NZ3 as various  
47  
48 108 grain sizes were available from that specific sample, collected from the loess profile  
49  
50 109 investigated by Brezeanu et al. (2021).

## 53 110 **3. Methodology**

### 56 111 *Sample preparation*

112 Stainless steel tubes were used for collecting the luminescence sample. The minerals  
113 of interest were extracted under subdued red light laboratory conditions. The  
114 material from the end of each tube was removed and used for gamma spectrometry  
115 measurements. The material from the inner part of the tube was used for 4-11  $\mu\text{m}$   
116 quartz and polymineral grains extraction. In the first step of sample preparation the  
117 calcium carbonates and the organic matter were removed by employing a treatment  
118 with hydrochloric acid (10% concentration) and hydrogen peroxide (10%  
119 concentration followed by 30%). Minerals with diameters smaller than 63 microns  
120 were separated by wet sieving. The fine (4-11  $\mu\text{m}$ ) polymineral mixture was  
121 obtained after Stoke's law settling followed by centrifugation in distilled water  
122 (**Frechen et al., 1996; Lang et al., 1996**). A 10 days treatment with hexafluorosilicic  
123 acid was employed in order to isolate the fine (4-11  $\mu\text{m}$ ) quartz fraction from the  
124 polymineral combination. The extraction procedure for quartz fractions larger than  
125 63  $\mu\text{m}$  (63-90  $\mu\text{m}$ , 90-125  $\mu\text{m}$ , 125-180  $\mu\text{m}$ , 180-250  $\mu\text{m}$ ) is described in **Brezeanu et**  
126 **al. (2021)**. Both fine quartz and polymineral grains were mounted on aluminium  
127 disks for luminescence measurements.

### 128 *Analytical Facilities*

129 Luminescence investigations were carried out using a Risø TL-OSL reader (model  
130 DA-20) equipped with an automated detection and stimulation head (DASH) (**Lapp**  
131 **et al., 2015**). The intensity of the blue (470 nm) and infrared (850 nm) LEDs deliver 80  
132 and 300 mW/cm<sup>2</sup>, respectively. Luminescence signals were detected by using PDM  
133 9107Q-AP-TTL-03 (160-630 nm) photomultiplier tubes (**Thomsen et al., 2006**).  
134 Quartz signals A 7.5-mm-thick Hoya U-340 UV filter was used for quartz signal  
135 determination while the polymineral signals were detected by using a blue filter  
136 combination (Schott BG39 + Corning 7-59, with transmission between 320 and 460  
137 nm). A radioactive source of <sup>90</sup>Sr-<sup>90</sup>Y was used for laboratory irradiation. The beta  
138 source was calibrated using gamma-irradiated calibration quartz (**Hansen et al.,**  
139 **2015**).

140 The polymineral fine grains aliquots used for residual dose and dose recovery  
141 measurements were exposed to window light under natural conditions in order to  
142 remove the natural signal.

143 ESR measurements were performed on an X band Bruker EMX Plus Spectrometer.  
144 All samples were placed in quartz glass tubes filled by maintaining the same  
145 volume, with a mass between 100 and 200 mg, and the measurements were  
146 normalized to 100 mg for inter-comparison. Each sample was measured 3 times and  
147 rotated in the cavity between the measurements. Exposure of samples to sunlight  
148 during measurements was restricted to a minimum. Measurements were carried out  
149 at 90 K (in liquid nitrogen) for Al-h and Ti centres, and at room temperature for E'  
150 and "peroxy" centres. Al-h and "peroxy" spectra were acquired using the following  
151 settings:  $3350 \pm 200$  G scanned magnetic field, modulation amplitude 1 G,  
152 modulation frequency 100 kHz, microwave power 2 mW, conversion time 50 ms,  
153 time constant 40 ms. For Ti measurements the settings were:  $3490 \pm 110$  G scanned  
154 magnetic field, modulation amplitude 1 G, modulation frequency 100 kHz,  
155 microwave power 10.0 mW, conversion time 10 ms, time constant 20.48 ms, and 10  
156 scans per measurement. For E' spectra the settings were:  $3363 \pm 10$  G scanned  
157 magnetic field, modulation amplitude 0.1 G, modulation frequency 100 kHz,  
158 microwave power 0.02 mW, conversion time 30 ms, time constant 20.48 ms, and 3  
159 scans per measurement. Baseline correction was performed using Bruker's Xenon  
160 software.

#### 161 *Equivalent dose determination*

162 Quartz equivalent dose determination has been carried out by using the standard  
163 Single Aliquot Regenerative dose (SAR) protocol (Murray and Wintle 2000, 2003)  
164 whereas polymineral fine grains equivalent doses were measured by applying two  
165 elevated temperature post-infrared infrared stimulation protocols, namely pIRIR<sub>225</sub>  
166 (Roberts 2008; Buylaert et al., 2009) and pIRIR<sub>290</sub> (Buylaert et al., 2011a; Thiel et al.,

167 **2011**). The protocols are outlined in **Table S1** while a more detailed description of  
168 the protocols is found in Supplementary material.

#### 169 *Dosimetry*

170 High-resolution gamma spectrometry was used for the specific radionuclide  
171 activities determination using a well-type HPGe detector. In order to reach the  
172 equilibrium of  $^{222}\text{Rn}$  with its parent  $^{226}\text{Ra}$ , samples were stored for 1 month before  
173 measurements. The annual dose rates were derived following the conversion factors  
174 tabulated by **Guérin et al. (2011)**. An alpha efficiency factor of  $0.04\pm 0.02$  was taken  
175 into account for 4-11  $\mu\text{m}$  quartz while for the polymineral fine grains the assumed  
176 alpha efficiency value was  $0.08\pm 0.02$  (**Rees-Jones, 1995**). The time averaged water  
177 content was assumed to be 15% with a relative error of 25%. The water content was  
178 chosen to represent the mean value of the sediment moisture over the entire  
179 depositional history. Similar values were used for dating sediments from Canterbury  
180 Plains and Banks Peninsula, respectively (**Rowan et al., 2012; Sohbati et al., 2016;**  
181 **Brezeanu et al., 2021**). The cosmic dose rate was estimated as function of depth,  
182 altitude and geomagnetic latitude using the formula proposed by **Prescott and**  
183 **Hutton (1994)**. Given the size of fine grains (4-11  $\mu\text{m}$ ), any dose rate derived from  
184 internal alpha activity was assumed to be negligible. The specific radionuclide  
185 activities and annual doses are presented in **Table 1**.

## 186 **4. Results and Discussion**

### 187 *Luminescence properties – Quartz*

188 Equivalent doses on fine quartz were determined by interpolating the sensitivity  
189 corrected natural OSL signal onto the dose response curve. **Figure 1** shows a  
190 representative SAR growth curve and OSL decay curves for a single aliquot of fine  
191 quartz extracted from sample NZ 7. The natural and regenerative OSL signal  
192 exhibits a similar pattern to the decay measured for calibration quartz during the  
193 first seconds of stimulation, which is accepted as being dominated by the fast

194 component (Hansen et al., 2015). The dose response curve was best described by a  
195 sum of two saturating exponential functions. Recycling and IR depletion ratios were  
196 within 10% deviation from unity which demonstrates that sensitivity corrections are  
197 properly made and the quartz signals are pure. Recuperation ratio was less than 2%  
198 indicating that the growth curves pass very close to the origin and thermal transfer  
199 during the repeated SAR cycle is negligible.

(Figure 1)

### Preheat plateau

202 The dependency of the equivalent doses on the preheat temperature was  
203 investigated through the preheat plateau test. Sample NZ 7 was divided in sets of  
204 five aliquots. For each set, a preheat temperature ranging from 180 to 280 °C was  
205 applied. A test dose cutheat of 180 °C was employed throughout the measurements.  
206 As can be seen from Figure S2, the equivalent doses do not display any significant  
207 variation over the investigated interval of preheat temperatures. The results of the  
208 intrinsic SAR tests were satisfactory for all the aliquots measured.

### Dose recovery test

210 Further, a dose recovery test has been performed on six samples (NZ 6, NZ 7, NZ 8,  
211 NZ 9, NZ 10 and NZ 11) in order to investigate whether the SAR protocol can  
212 successfully determine a known laboratory dose prior to any thermal treatment  
213 (Murray and Wintle, 2003). Sets of five aliquots from each sample were used. The  
214 natural signals were bleached by a repeated exposure to blue LEDs for 100 s at room  
215 temperature with a pause of 10 ks. The aliquots were irradiated with a beta dose  
216 chosen to approximate the natural dose and measured by using the SAR protocol in  
217 the same manner as measuring the equivalent dose. Figure S3 represents the results  
218 of the dose recovery test. As can be seen, the dose recovery results for all samples  
219 documented here were satisfactory indicating that the SAR protocol can successfully  
220 recover laboratory doses up to 46 Gy.



221 **Equivalent doses**

222 The measured quartz equivalent doses are summarized in **Table 1**. At least 10  
223 aliquots were measured for each sample in order to calculate the final equivalent  
224 dose.

225 The OSL equivalent doses range from  $1.3\pm 0.1$  Gy obtained for sample NZ 6 collected  
226 from a depth of 10 cm to  $46\pm 1$  Gy for sample NZ 11 which was collected from a  
227 depth of 109 cm.

228 **(Table 1)**

229 *Luminescence properties – Polymineral fine grains*

230 Equivalent doses measured on polymineral fine grains were determined by  
231 interpolating the natural sensitivity corrected IRSL signal onto the dose response  
232 curve constructed for each sample using both pIRIR protocols. **Figure 2** displays a  
233 representative growth curve of sample NZ 7 constructed by applying pIRIR<sub>225</sub>  
234 (**Figure 2a**) and pIRIR<sub>290</sub> (**Figure 2b**) protocols, respectively. A comparison between  
235 the decay curve of the natural signal and the pattern of a regenerative signal is  
236 shown in the insets of **Figure 2**. The dose response curves constructed using both  
237 pIRIR protocols were best fitted using a sum of two saturating exponential functions.  
238 The measured equivalent doses obtained on pIRIR<sub>225</sub> protocol range from  $7.5\pm 0.5$  Gy  
239 for the youngest sample NZ 6 to  $79\pm 2$  Gy for sample NZ 10. On the other hand,  
240 pIRIR<sub>290</sub> equivalent doses vary between  $23\pm 2$  Gy for sample NZ 6 and  $121\pm 5$  Gy for  
241 sample NZ10. pIRIR measured equivalent doses for each sample investigated here  
242 are labelled in **Table 1**.

243 **(Figure 2)**

244 **Residual doses**

245 It is well known that pIRIR signals are more difficult to be reset than OSL signals  
246 (e.g., Buylaert et al., 2009, 2012; Thiel et al., 2011). Many studies reported residual

1 247 doses of a few Grays obtained even after long exposure of the aliquots to sunlight or  
2 248 solar simulator (e.g., **Buylaert et al., 2011a, 2012; Stevens et al., 2011; Murray et al.,**  
3  
4 249 **2012; Yi et al., 2016, 2018; Avram et al., 2020; 2022; Brezeanu et al., 2021**). Moreover,  
5  
6 250 from long-term bleaching experiments using pIRIR<sub>290</sub> protocol **Yi et al. (2016, 2018)**  
7  
8 251 reported that for pIRIR<sub>290</sub> protocol, a constant residual dose of  $\sim 6 \pm 1$  Gy and  $\sim 4 \pm 1$  Gy  
9  
10 252 is achieved after 300 h beaching in solar simulator for samples collected from  
11  
12 253 Chinese loess. Based on the aforementioned information, the residual dose  
13  
14 254 corrections should be cautiously evaluated especially when dealing with young  
15  
16 255 samples.

17  
18  
19  
20 256 The assessment of the residual level has been made on five aliquots of each sample.  
21  
22 257 The natural signal has been erased by exposing the aliquots to sunlight for 30 days  
23  
24 258 prior to measurements. Residual doses obtained using pIRIR<sub>225</sub> protocol range from  
25  
26 259  $2.1 \pm 0.4$  Gy for the youngest sample with a measured equivalent dose of  $7.5 \pm 0.5$  Gy to  
27  
28 260  $3.2 \pm 0.3$  Gy for a sample with a measured equivalent dose of  $63 \pm 1$  Gy. On the other  
29  
30 261 hand, the pIRIR<sub>290</sub> residual doses vary from  $4 \pm 1$  Gy for the youngest sample with a  
31  
32 262 measured equivalent dose of  $23 \pm 2$  Gy to  $6.5 \pm 1$  Gy for a sample with a measured  
33  
34 263 equivalent dose of  $107 \pm 6$  Gy. The values obtained on each sample are displayed in  
35  
36 264 **Table S2**. Similar values of residual dose were obtained by **Brezeanu et al. (2021)** for  
37  
38 265 samples with comparable measured equivalent doses of  $\sim 84$  Gy and  $\sim 120$  Gy,  
39  
40 266 respectively. In their study, **Brezeanu et al. (2021)** reported that a constant residual  
41  
42 267 dose of  $\sim 4 \pm 1$  Gy has been reached after 48 h exposure to sunlight for pIRIR<sub>225</sub>  
43  
44 268 protocol while in the case of pIRIR<sub>290</sub> protocol, a constant level of  $\sim 10 \pm 1$  Gy was  
45  
46 269 achieved after 96 h of bleaching for New Zealand loess. They mentioned that such  
47  
48 270 values are in line with those measured after a 30 days exposure to sunlight.

49  
50  
51  
52  
53 271 Since it is still questionable whether the natural bleaching condition can be  
54  
55 272 thoroughly replicated in laboratory, it is advisable to use a modern analogue sample  
56  
57 273 for residual dose corrections, as well. In this case, the NZ 6 sample was used as a  
58  
59 274 modern sample. As such, an equivalent dose of  $7.5 \pm 0.5$  Gy was measured using  
60  
61  
62  
63  
64  
65

1 275 pIRIR<sub>225</sub> protocol and 22.8±1.5 Gy using pIRIR<sub>290</sub> protocol, respectively. Based on the  
2 276 laboratory residuals, we considered these values as the maximum residual doses.  
3  
4 277 Thus, the residual dose correction has been performed by using both laboratory and  
5  
6 278 modern analogue doses (**Table 1**).  
7

### 8 9 279 **Dose recovery test**

10  
11  
12 280 The reliability of the measurement protocols was achieved through a dose recovery  
13  
14 281 test (**Murray 1996; Wallinga et al., 2000**) on five aliquots from samples NZ 6, NZ 7  
15  
16 282 and NZ 8. The natural signals were removed by exposing the aliquots to window  
17  
18 283 light for 30 days. Then, the aliquots were irradiated with known laboratory doses  
19  
20 284 that were chosen to approximate the measured equivalent dose. To quantify the  
21  
22 285 accuracy of the protocols to measure laboratory given doses, a ratio between the  
23  
24 286 recovered and given dose was calculated. The results of the dose recovery tests for  
25  
26 287 both pIRIR protocols are showed in **Figure 3**. As can be seen, dose recovery ratios  
27  
28 288 obtained for pIRIR<sub>225</sub> protocol range from 0.98±0.02 for sample NZ 7 to 1.01±0.06 for  
29  
30 289 sample NZ 6 while the pIRIR<sub>290</sub> protocol dose recovery ratios vary from 1.07±0.06  
31  
32 290 obtained for sample NZ 6 to 1.23±0.05 calculated for sample NZ 8. These results  
33  
34 291 showed that pIRIR<sub>225</sub> protocol can successfully recover known doses over the dose  
35  
36 292 interval investigated here, while for pIRIR<sub>290</sub> protocol some degree of overestimation  
37  
38 293 is observed. A recent study conducted by **Avram et al. (2022)** showed that pIRIR<sub>290</sub>  
39  
40 294 dose recovery ratios overestimate unity between 12% and 46% for given doses that  
41  
42 295 range from ~100 Gy to ~850 Gy.  
43  
44  
45  
46

### 47 296 **(Figure 3)**

48  
49  
50 297 Some previous studies attributed the poor results of the pIRIR<sub>290</sub> dose recovery test  
51  
52 298 to the incorrect measurement of the residual dose (e.g., **Thomsen et al., 2008;**  
53  
54 299 **Buylaert et al., 2012**). In order to circumvent the potential contribution due to  
55  
56 300 inaccurate estimation for residual doses, a dose recovery test can be carried out by  
57  
58 301 adding laboratory beta doses on top of the natural dose. As such, dose recovery test  
59  
60  
61  
62  
63  
64  
65

1 302 results are further determined as a ratio between the measured dose and the sum of  
2 303 the natural and additional irradiated dose (equivalent dose + given dose on top)  
3  
4 304 (**Buylaert et al., 2011b; Yi et al., 2018**).

5  
6  
7 305 In this study, five aliquots from samples NZ 6 (measured  $De=23\pm 2$  Gy), NZ  
8  
9 306 7(measured  $De=111\pm 5$  Gy), NZ 8 (measured  $De=114\pm 5$  Gy) and NZ 9 (measured  
10  
11 307  $De=107\pm 6$  Gy) were irradiated on top of the natural signal with a beta dose of 100 Gy.  
12  
13 308 As such, for the total dose (natural+given dose) of 123 Gy (NZ 6) a dose recovery  
14  
15 309 ratio of  $1.08\pm 0.03$  was obtained whereas for sample NZ 8 with a total dose of 214 Gy  
16  
17  
18 310 was calculated a ratio of  $1.25\pm 0.06$ . The results for each sample are represented in  
19  
20 311 **Figure 3**. These results confirm our previous observation that in the case of pIRIR<sub>290</sub>  
21  
22 312 protocol, a dose overestimation is achieved.

### 23 24 25 313 **Fading**

26  
27  
28 314 Feldspars are known to suffer from anomalous fading phenomenon (**Wintle 1973;**  
29  
30 315 **Spooner 1992, 1994**), which is described as the luminescence signal loss under  
31  
32 316 ambient temperature. The percentage of the signal that was lost over a decade can be  
33  
34 317 quantified in term of fading rates (**Aitken 1985**).

35  
36  
37 318 The pIRIR<sub>290</sub> natural signal is considered to be a stable signal since **Thiel et al. (2011)**  
38  
39 319 reported for the first time that the natural pIRIR<sub>290</sub> signal for an old sample is in  
40  
41 320 saturation and thus the ages do not need any further fading corrections. Later, these  
42  
43 321 findings were also confirmed by other studies (e.g., **Stevens et al., 2011; Buylaert et**  
44  
45 322 **al., 2011a; Thomsen et al., 2011; Veres et al., 2018; Avram et al., 2020**).

46  
47  
48 323 To investigate the degree of signal loss for the pIRIR<sub>225</sub> natural signals, five aliquots  
49  
50 324 from sample NZ 7, NZ 9 and NZ 11 were used for fading measurements. The  
51  
52 325 aliquots used for this experiment were also used for dose recovery test. Firstly, each  
53  
54 326 aliquot from each sample was irradiated with a beta dose of 100 Gy. The test dose  
55  
56  
57 327 magnitude was kept as in the equivalent dose measurements. Four consecutive  
58  
59 328 reads-out were implied prior to the fading measurement. For each sample, different  
60  
61  
62  
63  
64  
65

329 storage time ranging between 2 h and 2 days were used. A preheat treatment was  
330 included prior to storage. The results of the fading test are presented in **Table S3**.  
331 For all samples, the variation of the measured fading rates for each aliquot is small.  
332 For sample NZ 7 a g-value of  $1.06\pm 0.16$  %/decade was measured whereas for sample  
333 NZ 11 the average measured fading rate was  $1.03\pm 0.28$ . On the other hand, a  
334 negative fading rate value of  $-0.04\pm 0.03$  was measured for sample NZ 9. Such low  
335 values for the fading rates are considered to be laboratory artefact (**Vasiliniuc et al.,**  
336 **2012**) and the pIRIR<sub>225</sub> ages do not need any correction for fading (**Avram et al., 2020;**  
337 **Brezeanu et al., 2021; Avram et al., 2022**). Therefore, in the further sections are  
338 discussed the uncorrected pIRIR ages.

#### 339 *ESR investigations*

340 As the poor luminescence properties of coarse quartz in the region are well known  
341 (**Preusser et al., 2006**) and were characterised in detail at a nearby site (**Brezeanu et**  
342 **al., 2021**), it is important to gain a better understanding of the intrinsic and extrinsic  
343 defects that exist in the fine fraction compared to the coarser fractions given that it  
344 was shown above that the first is amendable to the application of OSL dating, on the  
345 contrary to the latter. In this respect, ESR analysis have been performed on different  
346 grain sizes of quartz (4-11  $\mu\text{m}$ , 63-90  $\mu\text{m}$ , 90-125 $\mu\text{m}$ , 125-180 $\mu\text{m}$  and 180-250 $\mu\text{m}$ )  
347 extracted from sample NZ 3 which was collected from the nearby loess profile  
348 investigated by **Brezeanu et al. (2021)**, as this was the only sample from which  
349 sufficient amount of quartz of different grain sizes could be extracted for analysis.  
350 Luminescence properties of coarser fractions of quartz were thoroughly described in  
351 **Brezeanu et al. (2021)** while 4-11  $\mu\text{m}$  quartz fraction of sample NZ 3 presents similar  
352 luminescence characteristics as those displayed by the investigated samples from  
353 this study (NZ 6-NZ 12), and an equivalent dose of  $29\pm 3$  Gy was determined by  
354 measuring 8 aliquots.

355 **Figure 4** presents the ESR spectra of the different grain sizes of quartz compared  
356 to calibration quartz, a 180–250  $\mu\text{m}$  quartz fraction separated from aeolian sand from

357 Rømø, Jutland, Denmark, provided by Risø National Laboratory (Hansen et al.,  
358 2015) and investigated by ESR in Timar-Gabor (2018). No significant differences  
359 regarding the presence of paramagnetic species were observed between the  
360 investigated NZ3 sample and the calibration quartz.

361 (Figure 4)

362 The intensities of ESR signals were given in Table 2. The intensity of Al-h signal  
363 was determined from peak-to-peak amplitude measurements between the top of the  
364 first peak ( $g = 2.018$ ) to the bottom of the last peak ( $g = 1.993$ ) (Toyoda and  
365 Falguères, 2003). For the Ti centre the intensities were obtained using “options A, B  
366 and D” described in Duval and Guilarte (2015) and Duval et al. (2017), associated  
367 with a mixture of Ti-H and Ti-Li centers. Option A was measured from the top of  $g =$   
368 1.979 to the bottom of the peak around  $g = 1.913-1.915$ , option B as a peak-to-peak  
369 amplitude of the signal at  $g = 1.931$  and option D as a peak-to-baseline amplitude of  
370 the signal  $g = 1.913-1.915$ . The intensity of the E' signal was evaluated from the peak-  
371 to-peak height of the signal, and for “peroxy” signal it was determined from the  
372 peak-to-peak height from  $g \approx 2.003$  to  $g \approx 2.009$  (Odom and Rink, 1989).

373 (Table 2)

374 ESR spectra of Al-h centre (Figure 4a) show a significant contribution from the  
375 “peroxy” signal, which is relatively strong in these samples (Figure 4c). Al-h and  
376 “peroxy” signals are considerably stronger in 4-11  $\mu\text{m}$  quartz, compared to other  
377 fractions, about 3 and 4 times higher than in the case of 63-90  $\mu\text{m}$  fraction, for Al-h  
378 and “peroxy” respectively. Interestingly, Ti signals are very weak in all of the  
379 investigated samples, especially in the 4-11 $\mu\text{m}$  fraction (Figure 4b), for which the  
380 intensity amounts to 40-60% of the intensity observed for 63-90  $\mu\text{m}$  fraction. E' signal  
381 intensity in the smallest fraction is about 3 times bigger than in 63-90  $\mu\text{m}$  fraction,  
382 and reduces with increasing grain size (Figure 4d). General trends observed in the  
383 case of fine grains compared to the coarse ones – a higher intensity of Al-h, “peroxy”

384 and E' signals, as well as very low intensity of Ti centres, are the same as reported in  
385 **Timar-Gabor 2018** for samples which displayed a very good OSL behaviour (quartz  
386 from loess from Roxolany, Ukraine (**Anechitei-Deacu et al., 2018**) and Stayky,  
387 Ukraine (**Veres et al., 2018**). This suggests that the cause of the poor OSL properties  
388 of the investigated coarse grained quartz samples might be connected with some  
389 non-paramagnetic species, which cannot be detected by ESR spectroscopy.

## 390 5. Luminescence Ages

391 Luminescence ages obtained by using SAR-OSL protocol on fine quartz as well as  
392 pIRIR<sub>225</sub> and pIRIR<sub>290</sub> protocols, respectively, are presented in **Table 1** along with the  
393 dosimetry data. Only the pIRIR ages calculated with the modern analogue correction  
394 are discussed in this section.

395 Fine quartz luminescence ages range from  $0.3 \pm 0.04$  ka for sample NZ 6 which was  
396 collected from the uppermost part of the section to  $13 \pm 2$  ka for sample NZ 9.

397 The pIRIR<sub>225</sub> ages calculated using a residual dose correction based on the modern  
398 analogue sample range between  $14 \pm 1$  ka for sample NZ 7 and  $18 \pm 2$  ka for sample NZ  
399 9 for pIRIR<sub>225</sub> protocol. On the other hand, luminescence ages measured using  
400 pIRIR<sub>290</sub> protocol, vary from  $20 \pm 2$  ka for sample NZ 7 to  $27 \pm 3$  ka for sample NZ 9. As  
401 can be seen, the pIRIR<sub>290</sub> luminescence ages are slightly higher than those measured  
402 using pIRIR<sub>225</sub> protocol. Such age discrepancy between the two pIRIR protocols  
403 over this age interval has been previously observed in several studies, such as on  
404 European loess (**Zhang et al., 2018; Avram et al., 2020**) and on New Zealand loess  
405 (**Micallef et al., 2021; Brezeanu et al., 2021**), respectively.

406 The two sets of pIRIR ages calculated based on modern analogue correction along  
407 with the fine quartz SAR-OSL ages are presented in **Figure S4** as function of depth.  
408 An age reversal can be observed between sample NZ 9 and NZ 10, and occur  
409 between a depth of ~70 cm and ~130 cm. Such age reversal has been previously  
410 observed at the same depths from a nearby loess site by **Brezeanu et al. (2021)** as

1  
2 411 well as by others in the Canterbury region (e.g., **Berger et al., 2001; Almond et al.,**  
3 412 **2007; Rowan et al., 2012**).

4  
5 413 As can be seen from **Figure S4**, an age discrepancy between the three sets of ages is  
6  
7 414 displayed. Based on dose recovery test results as well as on the previous findings  
8  
9 415 (e.g., **Veres et al., 2018; Avram et al., 2020; 2022**), we interpret the pIRIR<sub>290</sub> ages as  
10  
11 416 being overestimated. Moreover, the SAR-OSL fine quartz and pIRIR<sub>225</sub> ages are not  
12  
13 417 in agreement even though the behaviour in the SAR procedure was satisfactory for  
14  
15 418 both minerals. The pIRIR<sub>225</sub> age for sample NZ 7 (14±1 ka) collected from a depth of  
16  
17 419 30 cm is similar with that obtained by **Brezeanu et al. (2021)** for sample NZ 2 (14±1  
18  
19 420 ka) which was collected from the same depth. Such overlapping was also found for  
20  
21 421 samples collected from a depth of ~50 and ~130 cm, respectively. As there is  
22  
23 422 evidence that reliable age up to ~50 ka can be obtained on fine quartz (e.g., **Timar-**  
24  
25 423 **Gabor and Wintle 2013., Avram et al., 2020**), the differences between the OSL and  
26  
27 424 pIRIR<sub>225</sub> ages reported here require further investigations.  
28  
29  
30

31 425

## 32 33 34 426 **6. Summary and Conclusions**

35  
36  
37 427 In this study the SAR-OSL protocol has been applied for the first time on fine quartz  
38  
39 428 alongside pIRIR<sub>225</sub> and pIRIR<sub>290</sub> protocols on polymineral fine grains for dating seven  
40  
41 429 samples of loess from an exposure in Southern Canterbury Plains South Island of  
42  
43 430 New Zealand. Luminescence behaviour of fine quartz in the SAR procedure was  
44  
45 431 investigated in the regard of IR depletion test, preheat plateau test and dose recovery  
46  
47 432 tests, respectively. The satisfactory results that have been obtained for all the  
48  
49 433 investigated tests have led to obtaining for the first-time fine quartz luminescence  
50  
51 434 ages for the investigated loess profile. Moreover, two sets of pIRIR ages have been  
52  
53 435 also determined on polymineral fine grains extracted from the same samples. All  
54  
55 436 three sets of ages range up to 13 ±2 ka (fine quartz), 18±2 ka (pIRIR<sub>225</sub>) and 27±3 ka  
56  
57 437 (pIRIR<sub>290</sub>), respectively suggesting that loess from the investigated profile was  
58  
59  
60  
61  
62  
63  
64  
65



1 438 accumulated during the last glacial maximum. As coarse quartz fractions were not  
2 439 amendable for OSL dating ESR investigations were performed on different grain  
3  
4 440 sizes of quartz. The main ESR impurity defects (Al and Ti centres) as well as the  
5  
6 441 most dominant intrinsic defects (E' and "peroxy") showed trends similar to those  
7  
8 442 previously reported for samples characterised by a very good OSL behaviour,  
9  
10 443 namely a higher intensity of Al-h, "peroxy" and E' signals, and much lower intensity  
11  
12 444 of Ti signals observed in the case of fine grains compared to the coarse grains. The  
13  
14 445 lack of significant differences in ESR signals between the samples suitable for OSL  
15  
16 446 dating such as calibration quartz and other samples previously investigated and the  
17  
18 447 New Zealand samples which display a poor luminescence behaviour suggest that  
19  
20 448 the factors leading to the different OSL characteristics might be connected with some  
21  
22 449 non-paramagnetic species, which cannot be detected by ESR spectroscopy.  
23  
24  
25

26 450

## 27 451 **Acknowledgements**

28  
29 452 This study was funded by the European Research Council (ERC) under the  
30  
31  
32 453 European Union's Horizon 2020 research and innovation programme ERC-2015-STG  
33  
34 454 (grant agreement No [678106]).  
35  
36  
37

38  
39 455 A. Avram and A. Timar-Gabor, acknowledge the financial support of the research  
40  
41 456 project EEA-RO-NO-2018-0126.  
42  
43

44 457 A. Micallef acknowledges the financial support from the European Research Council  
45  
46 458 (ERC) under the European Union's Horizon 2020 research and innovation  
47  
48 459 programme (grant MARCAN 677898).  
49  
50

51 460

## 52 461 **References**

53  
54  
55  
56  
57 462 Aitken, M.J., Alldred, J.C., 1972. The assessment of error limits in thermoluminescent  
58  
59 463 dating. *Archaeometry* 14, 257-267.  
60  
61  
62  
63  
64  
65

- 464 Aitken, M.J., 1985. Thermoluminescence Dating. Academic Press, London, p. 360.
- 465 Alloway B.V., Lowe D.J., Barrell D.J.A., Newnham R.M., Almond P.C., Augustinus  
466 P.C., Bertler N.A.N., Carter L., Litchfield N.J., McGlone M.S., Shulmeister J.,  
467 Vandergoes M., Williams P. and NZ-INTIMATE Members, 2007. Towards a  
468 climate event stratigraphy for New Zealand over the past 30 000 years (NZ-  
469 INTIMATE project). *Journal of Quaternary Science* 22(1): 9-35,  
470 <https://onlinelibrary.wiley.com/doi/abs/10.1002/jqs.1079>
- 471 Almond PC, Moar NT and Lian OB, 2001. Reinterpretation of the glacial chronology  
472 of South Westland, New Zealand. *New Zealand Journal of Geology and*  
473 *Geophysics* 44, 1-15, <https://doi.org/10.1080/00288306.2001.9514917>.
- 474 Almond PC, Shanhun FL, Rieser U and Shulmeister J, 2007. An OSL, radiocarbon  
475 and tephra isochron-based chronology for Birdlings Flat loess at Ahuriri  
476 Quarry, Banks Peninsula, Canterbury, New Zealand. *Quaternary*  
477 *Geochronology* 2: 4–8, <http://dx.doi.org/10.1016/j.quageo.2006.06.002>
- 478 Anechitei-Deacu, V., Timar-Gabor, A., Constantin, D., Trandafir-Anothi, O., Del  
479 Valle, L., Fornos, J.J., Gomez-Pujol, L., Wintle, A.G., 2018. Assessing the  
480 maximum limit of SAR-OSL dating using quartz of different grain sizes.  
481 *Geochronometria* 45, 146-159. <http://dx.doi.org/10.1515/geochr-2015-0092>
- 482 Avram A, Constantin D, Veres D, Kelemen S, Obreht I, Hambach U, Marković SB  
483 and Timar-Gabor A, 2020. Testing polymineral post-IR IRSL and quartz SAR-  
484 OSL protocols on Middle to Late Pleistocene loess at Batajnica, Serbia. *Boreas*  
485 49: 615-63. <https://onlinelibrary.wiley.com/doi/full/10.1111/bor.12442>.
- 486 Avram, A., Constantin, D., Hao, Q., Timar-Gabor, A., 2022. Optically stimulated  
487 luminescence dating of loess in South-Eastern China using quartz and  
488 polymineral fine grains. *Quaternary Geochronology* 67, 101226.  
489 <http://dx.doi.org/10.1016/j.quageo.2021.101226>

- 1  
2  
3  
4  
5  
6  
7  
8  
9  
10  
11  
12  
13  
14  
15  
16  
17  
18  
19  
20  
21  
22  
23  
24  
25  
26  
27  
28  
29  
30  
31  
32  
33  
34  
35  
36  
37  
38  
39  
40  
41  
42  
43  
44  
45  
46  
47  
48  
49  
50  
51  
52  
53  
54  
55  
56  
57  
58  
59  
60  
61  
62  
63  
64  
65
- 490 Berger GW, Pillans BJ., Tonkin PJ, 2001. Luminescence chronology of loess-paleosol  
491 sequences from Canterbury, South Island, New Zealand. *New Zealand Journal*  
492 *of Geology and Gheophysics* 44, 501-516,  
493 <https://doi.org/10.1080/00288306.2001.9514952>
- 494 Berger GW, Pillans BJ, Bruce JG and McIntosh PD, 2002. Luminescence chronology  
495 of loess-paleosol sequences from southern South Island, New Zealand.  
496 *Quaternary Science Reviews* 21, 1899-1913, [10.1016/S0277-3791\(02\)00021-5](https://doi.org/10.1016/S0277-3791(02)00021-5).
- 497 Bösken, J., Klasen, N., Zeeden, C., Obreht, I., Marković, S.B., Hambach, U.,  
498 Lehmkuhl, F., 2017. New luminescence-based geochronology framing the last  
499 two glacial cycles at the southern limit of European Pleistocene loess in Stalać  
500 (Serbia). *Geochronometria* 44, 150-161. <http://dx.doi.org/10.1515/geochr-2015-0062>.
- 501  
502 Buylaert JP, Murray AS and Thomsen KJ, 2009. Testing the potential of an elevated  
503 temperature IRSL signal from K-feldspar. *Radiation Measurements* 44, 560–565,  
504 <https://doi.org/10.1016/j.radmeas.2009.02.007>.
- 505 Buylaert J.P., Huot S., Murray A.S., Van Den Haute P., 2011a. Infrared stimulated  
506 luminescence dating of an Eemian (MIS 5e) site in Denmark using K-feldspar.  
507 *Boreas* 40, 46–56, <https://doi.org/10.1111/j.1502-3885.2010.00156.x>.
- 508 Buylaert J.P., Thiel, C., Murray, A., Vandenberghe, S., Yi, S., Lu, H., 2011b. IRSL and  
509 post-IR IRSL residual doses recorded in modern dust samples from the  
510 Chinese loess plateau. *Geochronometria* 38, 432-440.  
511 <http://dx.doi.org/10.2478/s13386-011-0047-0>.
- 512 Buylaert, J.-P., Jain, M., Murray, A.S., Thomsen, K.J., Thiel, C., Sohbaty, R., 2012. A  
513 robust feldspar luminescence dating method for Middle and Late Pleistocene  
514 sediments. *Boreas* 41, 435–451. <https://doi.org/10.1111/j.1502-3885.2012.00248.x>.

- 1  
2  
3  
4  
5  
6  
7  
8  
9  
10  
11  
12  
13  
14  
15  
16  
17  
18  
19  
20  
21  
22  
23  
24  
25  
26  
27  
28  
29  
30  
31  
32  
33  
34  
35  
36  
37  
38  
39  
40  
41  
42  
43  
44  
45  
46  
47  
48  
49  
50  
51  
52  
53  
54  
55  
56  
57  
58  
59  
60  
61  
62  
63  
64  
65
- 516 Brezeanu, D., Avram, A., Micallef, A., CintaPinzaru, S., Timar-Gabor, A., 2021.  
517 Investigations on the luminescence properties of quartz and feldspars  
518 extracted from loess in the Canterbury Plains, New Zealand South Island.  
519 *Geochronometria* 48, 46-60. <http://dx.doi.org/10.2478/geochr-2021-0005>.
- 520 Duval, M., Guilarte, V., 2015. ESR dosimetry of optically bleached quartz grains  
521 extracted from Plio-Quaternary sediment: Evaluating some key aspects of the  
522 ESR signals associated to the Ti-centers. *Radiation Measurements*, 78, 28–41.  
523 <https://doi.org/10.1016/j.radmeas.2014.10.002>
- 524 Duval, M., Arnold, L.J., Guilarte, V., Demuro, M., Santonja, M., Pérez-González, A.,  
525 2017. Electron spin resonance dating of optically bleached quartz grains from  
526 the Middle Palaeolithic site of Cuesta de la Bajada (Spain) using the multiple  
527 centres approach. *Quaternary Geochronology*, 37, 82–96.  
528 <https://doi.org/10.1016/j.quageo.2016.09.006>
- 529 Frechen M, Schweitzer U and Zander A, 1996. Improvements in sample preparation  
530 for the fine grain technique. *Ancient TL* 14, 15–17
- 531 Guérin G, Mercier N and Adamiec G, 2011. Dose-rate conversion factors: update.  
532 *Ancient TL* 29, 5–8.
- 533 Hansen V, Murray A, Buylaert JP, Yeo EY and Thomsen K, 2015. A new irradiated  
534 quartz for beta source calibration. *Radiation Measurements* 81, 123–127,  
535 <https://doi.org/10.1016/j.radmeas.2015.02.017>.
- 536 Hornblow. S., Quigley. M., Nicol A., Van Dissen, R., Wang, N., 2014.  
537 Paleoseismology of the 2010 Mw 7.1 Darfield (Canterbury) earthquake source,  
538 Greendale Fault, New Zealand. *Tectonophysics* 637. 178–190.  
539 <https://doi.org/10.1016/j.tecto.2014.10.004>.
- 540 Holdaway RN, Roberts RG, Beavan-Athfield NR, Olley JM and Worthy TH, 2002.  
541 Optical dating of quartz sediments and accelerator mass spectrometry 14C  
542 dating of bone gelatin and moa eggshell: a comparison of age estimates for

- 543 non-archaeological deposits in New Zealand. *Journal of the Royal Society of New*  
1  
2 544 *Zealand* 32, 463-505, <https://doi.org/10.1080/03014223.2002.9517705>.  
3  
4  
5 545 Hormes A, Preusser F, Denton G, Hajdas I, Weiss D, Stocker TF and Schlüchter C,  
6  
7 546 2003. Radiocarbon and luminescence dating of overbank deposits in outwash  
8  
9 547 sediments of the Last Glacial Maximum in North Westland, New Zealand.  
10  
11 548 *New Zealand Journal of Geology and Geophysics* 46, 95-106,  
12  
13 549 <https://doi.org/10.1080/00288306.2003.9514998>  
14  
15  
16 550 Lapp T, Kook M, Murray AS, Thomsen KJ, Buylaert JP and Jain M, 2015. A new  
17  
18 551 luminescence detection and stimulation head for the Risø TL/OSL reader.  
19  
20 552 *Radiation Measurements* 81, 178–184,  
21  
22 553 <https://doi.org/10.1016/j.radmeas.2015.02.001>.  
23  
24  
25 554 Lang A, Lindauer S, Kuhn R and Wagner GA, 1996. Procedures used for optically  
26  
27 555 and infrared stimulated luminescence dating of sediments in Heidelberg.  
28  
29 556 *Ancient TL* 14, 7–11  
30  
31  
32 557 Litchfield NJ and Rieser U, 2005. Optically stimulated luminescence age constraints  
33  
34 558 for fluvial aggradation terraces and loess in the eastern North Island, New  
35  
36 559 Zealand. *New Zealand Journal of Geology and Geophysics* 48, 581-589,  
37  
38 560 <https://doi.org/10.1080/00288306.2005.9515135>.  
39  
40  
41 561 Micallef, A., Marchis, R., Saadatkhah, N., Pondthai, P., Everett, M.E., Avram, A.,  
42  
43 562 Timar-Gabor, A., Cohen, D., Preca Trapani, R., Weymer, B.A., Wernette, P.,  
44  
45 563 2021. Groundwater erosion of coastal gullies along the Canterbury coast (New  
46  
47 564 Zealand): a rapid and episodic process controlled by rainfall intensity and  
48  
49 565 substrate variability. *Earth Surface Dynamics* 9, 1-18.  
50  
51 566 <https://doi.org/10.5194/esurf-9-1-2021>  
52  
53  
54 567 Murray AS, 1996. Developments in optically stimulated luminescence and photo-  
55  
56 568 transferred thermoluminescence dating of young sediments: application to a  
57  
58  
59  
60  
61  
62  
63  
64  
65

- 569 2000-years of flood deposits. *Geochimica et Cosmochimica Acta* 60, 565–576,  
1  
2 570 [https://doi.org/10.1016/0016-7037\(95\)00418-1](https://doi.org/10.1016/0016-7037(95)00418-1).  
3  
4  
5 571 Murray AS and Wintle AG, 2000. Luminescence dating using an improved single-  
6  
7 572 aliquot regenerative-dose protocol. *Radiation Measurements* 32, 57–73,  
8  
9 573 [https://doi.org/10.1016/S1350-4487\(99\)00253-X](https://doi.org/10.1016/S1350-4487(99)00253-X).  
10  
11  
12 574 Murray AS and Wintle AG, 2003. The single aliquot regenerative dose protocol:  
13  
14 575 potential for improvements in reliability. *Radiation Measurements* 37, 377–381,  
15  
16 576 [https://doi.org/10.1016/S1350-4487\(03\)00053-2](https://doi.org/10.1016/S1350-4487(03)00053-2).  
17  
18  
19 577 Murray AS, Thomsen KJ, Masuda N, Buylaert JP and Jain M, 2012. Identifying well-  
20  
21 578 bleached quartz using the different bleaching rates of quartz and feldspar  
22  
23 579 luminescence signals. *Radiation Measurements* 47, 688–695,  
24  
25 580 <https://doi.org/10.1016/j.radmeas.2012.05.006>.  
26  
27  
28 581 Nichol SL, Lian OB and Carter CH, 2003. Sheet-gravel evidence for a late Holocene  
29  
30 582 tsunami run-up on beach dunes, Great Barrier Island, New Zealand.  
31  
32 583 *Sedimentary Geology* 155, 129-145.  
33  
34  
35 584 Odom, A.L., Rink, W. J., 1989. Natural accumulation of Schottky-Frenkel defects:  
36  
37 585 Implications for a quartz geochronometer. *Geology*, 17(1), 55–58.  
38  
39 586 [https://doi.org/10.1130/0091-7613\(1988\)017<0055:NAOSFD>2.3.CO;2](https://doi.org/10.1130/0091-7613(1988)017<0055:NAOSFD>2.3.CO;2)  
40  
41  
42 587 Prescott JR and Hutton JT, 1994. Cosmic ray contributions to dose rates for  
43  
44 588 luminescence and ESR dating: large depths and long term variations.  
45  
46 589 *Radiation Measurements* 23, 497–500, [https://doi.org/10.1016/1350-](https://doi.org/10.1016/1350-4487(94)90086-8)  
47  
48 590 [4487\(94\)90086-8](https://doi.org/10.1016/1350-4487(94)90086-8).  
49  
50  
51 591 Preusser F, Andersen BG, Denton GH and Schlüchter C, 2005. Luminescence  
52  
53 592 chronology of Late Pleistocene glacial deposits in northWestland, New  
54  
55 593 Zealand. *Quaternary Science Reviews* 24, 2207-2227,  
56  
57 594 [10.1016/j.quascirev.2004.12.005](https://doi.org/10.1016/j.quascirev.2004.12.005).  
58  
59  
60  
61  
62  
63  
64  
65

- 1  
2  
3  
4  
5  
6  
7  
8  
9  
10  
11  
12  
13  
14  
15  
16  
17  
18  
19  
20  
21  
22  
23  
24  
25  
26  
27  
28  
29  
30  
31  
32  
33  
34  
35  
36  
37  
38  
39  
40  
41  
42  
43  
44  
45  
46  
47  
48  
49  
50  
51  
52  
53  
54  
55  
56  
57  
58  
59  
60  
61  
62  
63  
64  
65
- 595 Preusser F, Ramseyer K and Schlüchter C, 2006. Characterisation of low OSL  
596 intensity quartz from the New Zealand Alps. *Radiation Measurements* 41, 871-  
597 877, <https://doi.org/10.1016/j.radmeas.2006.04.019>.
- 598 Rees-Jones J, 1995. Optical dating of young sediments using fine-grain quartz.  
599 *Ancient TL* 13, 9–13.
- 600 Roberts H, 2008. The development and application of luminescence dating to loess  
601 deposits: a perspective on the past, present and future. *Boreas* 37, 483–507,  
602 <https://doi.org/10.1111/j.1502-3885.2008.00057.x>.
- 603 Roberts HM. 2015. Luminescence Dating, Loess. In *Encyclopedia of Scientific Dating*  
604 *Methods*, Rink WJ, Thompson JW (eds). Springer; 425–430.
- 605 Rowan AV, Roberts HM, Jones MA, Duller GAT, Covey-Crump SJ and Brocklehurst  
606 SH, 2012. Optically stimulated luminescence dating of glaciofluvial sediments  
607 on the Canterbury Plains, South Island, New Zealand. *Quaternary*  
608 *Geochronology* 8: 10-22, <https://doi.org/10.1016/j.quageo.2011.11.013>.
- 609 Rother H, Shulmeister J and Rieser U, 2009. Stratigraphy, optical dating chronology  
610 (IRSL) and depositional model of pre-LGM glacial deposits in the Hope  
611 Valley, New Zealand. *Quaternary Science Reviews*, 1-17,  
612 [10.1016/j.quascirev.2009.11.001](https://doi.org/10.1016/j.quascirev.2009.11.001).
- 613 Shulmeister, J., Thackray, G.D., Rieser, U., Hyatt, O.M., Rother, H., Smart, C.C.,  
614 Evans, D.J., 2010. The stratigraphy, timing and climatic implications of  
615 glaciolacustrine deposits in the middle Rakaia Valley, South Island, New  
616 Zealand. *Quaternary Science Reviews* 29, 2362-2381.  
617 <https://doi.org/10.1016/j.quascirev.2010.06.004>.
- 618 Sohbaty R, Borella J, Murray A, Quigley M and Buylaert JP, 2016. Optical dating of  
619 loessic hillslope sediments constrains timing of prehistoric rockfall,  
620 Christchurch, New Zealand. *Journal of Quaternary Science* 31: 678-690,  
621 <https://doi.org/10.1002/jqs.2895>.

- 622 Stevens T, Marković SB, Zech M, Hambach U and Sümegei P, 2011. Dust deposition  
623 and climate in the Carpathian Basin over an independently dated last glacial-  
624 interglacial cycle. *Quaternary Science Reviews* 30, 662–681,  
625 <https://doi.org/10.1016/j.quascirev.2010.12.011>.
- 626 Spooner, N.A., 1992. Optical dating—preliminary-results on the anomalous fading of  
627 luminescence from feldspars. *Quat. Sci. Rev.* 11, 139–145.  
628 [https://doi.org/10.1016/0277-3791\(92\)90055-D](https://doi.org/10.1016/0277-3791(92)90055-D).
- 629 Spooner, N.A., 1994. The anomalous fading of infrared-stimulated luminescence  
630 from feldspars. *Radiat. Meas.* 23, 625–632. [https://doi.org/10.1016/1350-4487\(94\)90111-2](https://doi.org/10.1016/1350-4487(94)90111-2).
- 632 Thiel C, Buylaert JP, Murray A, Terhorst B, Hofer I, Tsukamoto S and Frechen M,  
633 2011. Luminescence dating of the Stratzing loess profile (Austria) – Testing  
634 the potential of an elevated temperature post-IR IRSL protocol. *Quaternary  
635 International* 234, 23–31, <https://doi.org/10.1016/j.quaint.2010.05.018>.
- 636 Thomsen, K.J., Bøtter-Jensen, L., Denby, P.M., Moska, P., Murray, A.S., 2006.  
637 Developments in luminescence measurement techniques. *Radiat. Meas.* 41,  
638 768–773. <https://doi.org/10.1016/j.radmeas.2006.06.010>.
- 639 Thomsen K.J., Murray, A.S., Jain, M., 2011. Stability of IRSL signals from  
640 sedimentary K-feldspar samples. *Geochronometria* 38, 1-13.  
641 <http://dx.doi.org/10.2478/s13386-011-0003-z>.
- 642 Timar-Gabor, A., Wintle, A.G., 2013. On natural and laboratory generated dose  
643 response curves for quartz of different grain sizes from Romanian loess.  
644 *Quaternary geochronology* 18, 34-40.  
645 <http://dx.doi.org/10.1016/j.quageo.2013.08.001>.
- 646 Timar-Gabor, A., 2018. Electron spin resonance characterisation of sedimentary  
647 quartz of different grain sizes, *Radiation Measurements* 120, 59-65.  
648 <https://doi.org/10.1016/j.radmeas.2018.06.023>.



- 649 Toyoda, S., Falguères, C., 2003. The method to represent the ESR signal intensity of  
650 the aluminum hole center in quartz for the purpose of dating. *Advances in*  
651 *ESR Applications*, 20, 7–10.
- 652 Veres D, Tecsá V, Gerasimenko N, Zeeden C, Hambach U and Timar-Gabor A, 2018.  
653 Short-term soil formation events in last glacial east European loess, evidence  
654 from multi-method luminescence dating. *Quaternary Science Reviews* 200, 34–  
655 51, <https://doi.org/10.1016/j.quascirev.2018.09.037>.
- 656 Vasiliniuc, Ş., Vandenberghe, D.A.G., Timar-Gabor, A., Panaiotu, C., Cosma, C.,  
657 2012. Testing the potential of elevated temperature post-IR IRSL signals for  
658 dating Romanian loess. *Quaternary Geochronology* 10, 75-80.  
659 <http://dx.doi.org/10.1016/j.quageo.2012.02.014>.
- 660 Wallinga J, Murray A and Duller G, 2000. Underestimation of equivalent dose in  
661 single-aliquot optical dating of feldspars caused by preheating. *Radiation*  
662 *Measurements* 32, 691–695, [https://doi.org/10.1016/S1350-4487\(00\)00127-X](https://doi.org/10.1016/S1350-4487(00)00127-X).
- 663 Wintle, A.G., 1973. Anomalous fading of thermoluminescence in mineral samples.  
664 *Nature* 245, 143–144. <https://doi.org/10.1038/245143a0>.
- 665 Yi S, Buylaert JP, Murray AS, Lu H, Thiel C and Zeng L, 2016. A detailed post-IR  
666 IRSL dating study of the Niuyangzigou loess site in northeastern China.  
667 *Boreas* 45, 644–657, <https://doi.org/10.1111/bor.12185>.
- 668 Yi S, Li X, Han Z, Lu H, Liu J and Wu J, 2018. High resolution luminescence  
669 chronology for Xiashu Loess deposits of Southern China. *Journal of Asian Earth*  
670 *Sciences* 155: 188-197, <https://doi.org/10.1016/j.jseaes.2017.11.027>.
- 671 Yates K, Fenton CH and Bell DH, 2018. A review of the geotechnical characteristics  
672 of loess and loess-derived soils from Canterbury, South Island, New Zealand.  
673 *Engineering Geology* 236: 11-21, <https://doi.org/10.1016/j.enggeo.2017.08.001>.
- 674 Zhang, J., Rolf, C., Wacha, L., Tsukamoto, S., Durn, G., Frechen, M., 2018.  
675 Luminescence dating and palaeomagnetic age constraint of a last glacial loess-

676

paleosol sequence from Istria, Croatia. Quaternary International 494, 19-33.

1

2 677

3

<http://dx.doi.org/10.1016/j.quaint.2018.05.045>.

4 678

5

6

7

8

9

10

11

12

13

14

15

16

17

18

19

20

21

22

23

24

25

26

27

28

29

30

31

32

33

34

35

36

37

38

39

40

41

42

43

44

45

46

47

48

49

50

51

52

53

54

55

56

57

58

59

60

61

62

63

64

65

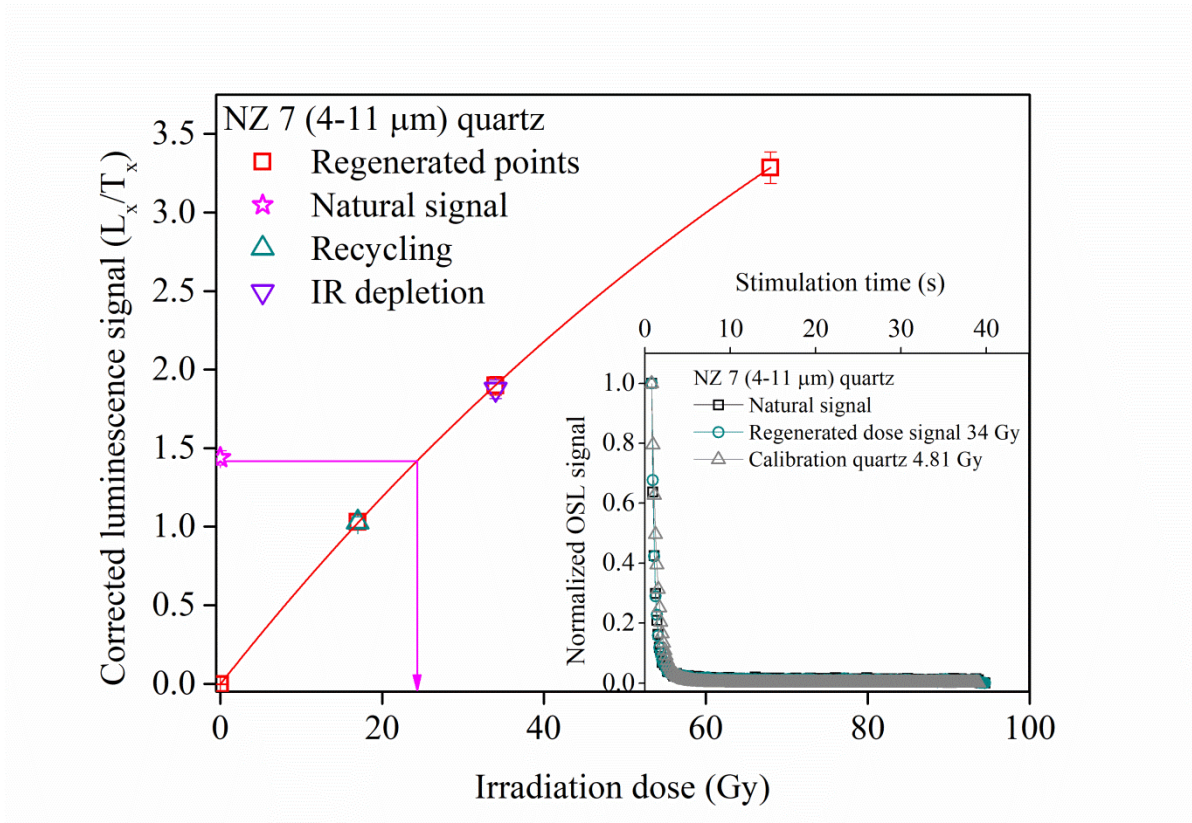


**Figure 1.** Representative sensitivity-corrected dose response curve constructed for one aliquot of sample NZ 7 on 4-11  $\mu\text{m}$  quartz using SAR-OSL protocol. The sensitivity corrected natural signals (stars) are interpolated on the dose response curves. IR depletion point is presented as an up triangle while the recycling points are presented as inverse triangles. The inset shows the pattern of a typical quartz decay curve which is compared with the decay of a regenerative dose as well as with the OSL decay of calibration quartz.

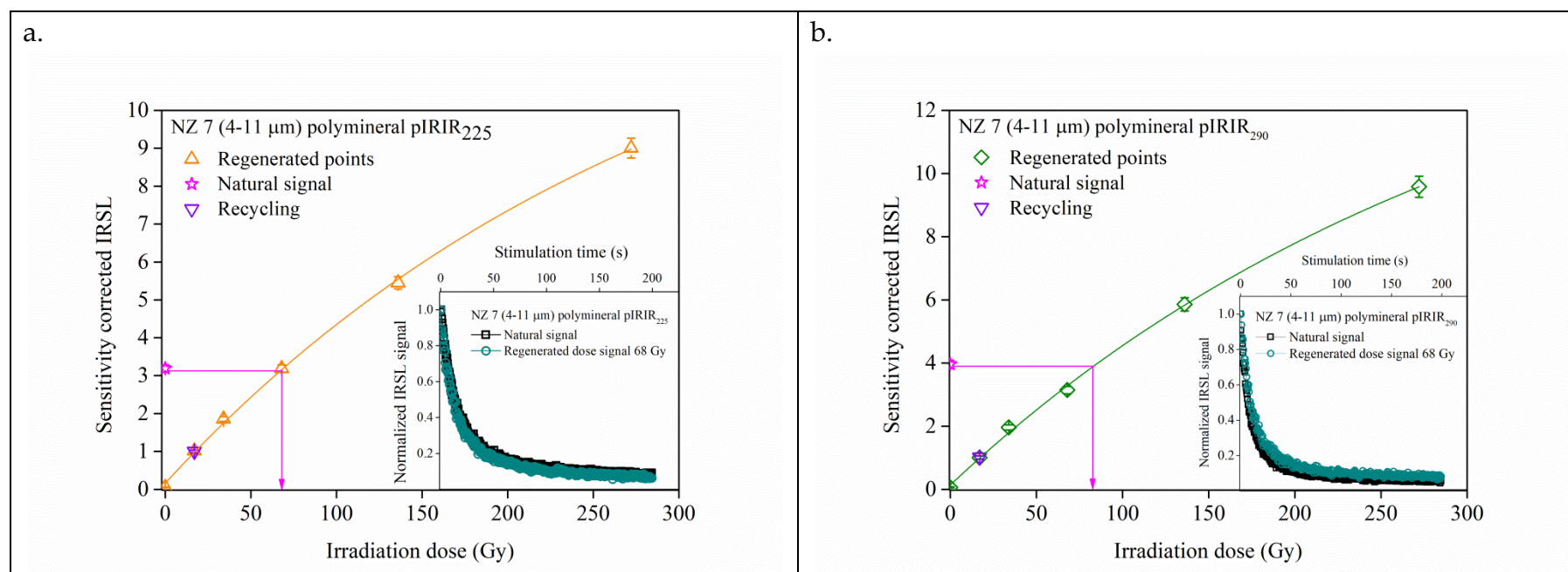


**Figure 2.** Representative sensitivity-corrected dose response curves constructed for one aliquot of sample NZ 7 on (a) 4-11  $\mu\text{m}$  polymineral fine grains using the pIRIR<sub>225</sub> protocol and (b) 4-11  $\mu\text{m}$  polymineral using pIRIR<sub>290</sub> protocol. The sensitivity corrected natural signals (stars) are interpolated on the dose response curves. The recycling points are presented as inverse triangles. Insets show typical decay curves. For polymineral fine grains, the natural CW-OSL signals are compared to regenerated signals induced by a beta dose approximately equal to the equivalent dose.

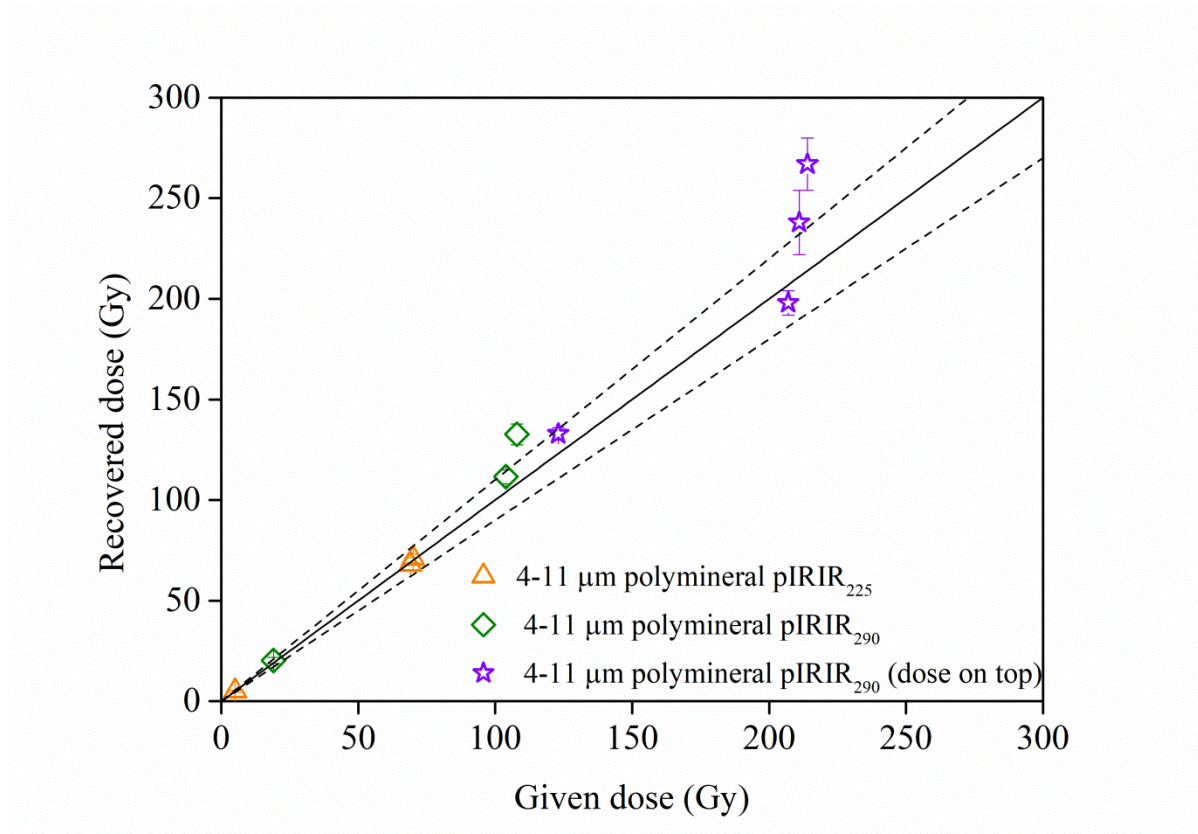


**Figure 3.** The results of dose recovery test using pIRIR<sub>225</sub> protocol (up triangle) and pIRIR<sub>290</sub> protocol (diamond symbol) on 4-11 μm polymineral aliquots from sample NZ 6, NZ 7 and NZ 8. Dose recovery test result when 100 Gy was added on top of the natural signal of sample NZ 6, NZ 7, NZ 8 and NZ 9 are depicted with a star symbol.

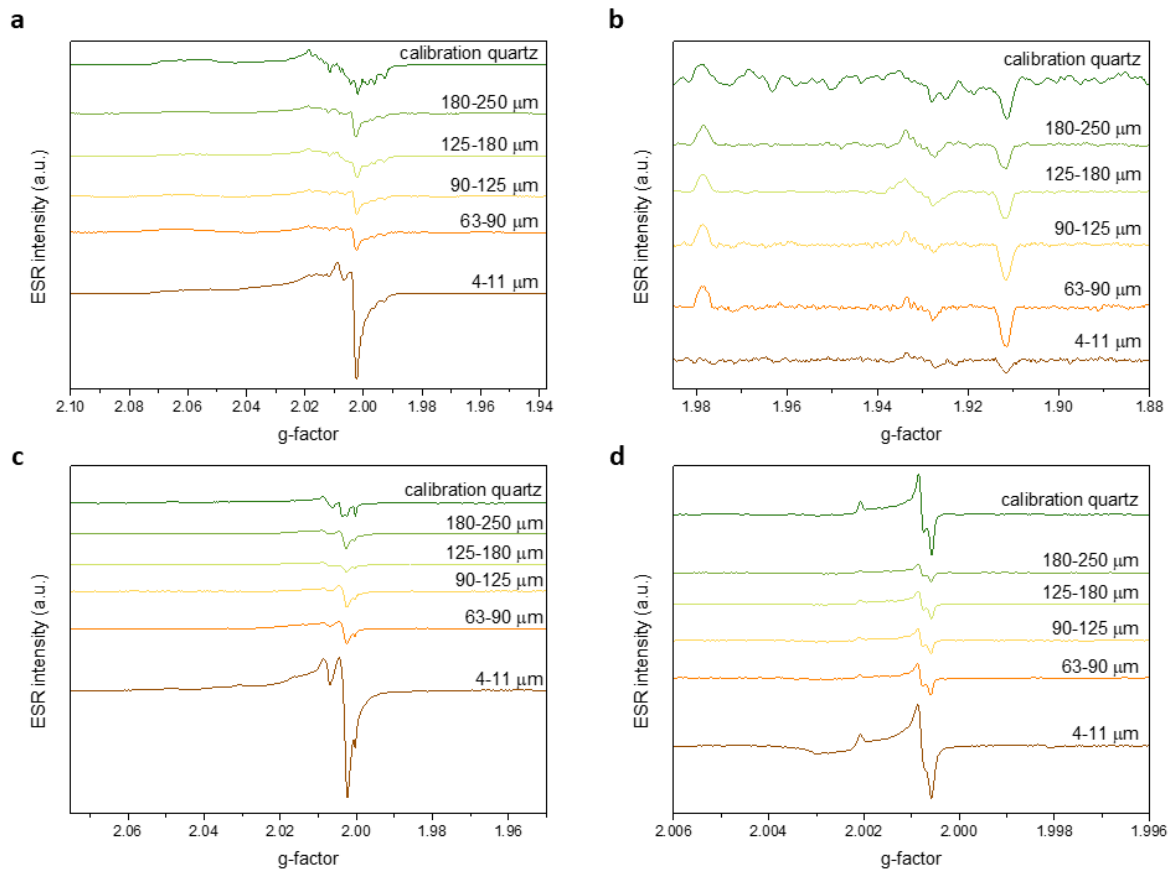


**Figure 4.** ESR spectra of Al-h (a), Ti (b), "peroxy" (c), and E' (d) centres, for quartz fractions 4-11, 63-90, 90-125, 125-180, 180-250  $\mu\text{m}$  from sample NZ 3, and for calibration quartz.

**Table 1.** Summary of the SAR-OSL, pIRIR<sub>225</sub> and pIRIR<sub>290</sub> luminescence ages. The age uncertainties were determined following **Aitken and Aldred (1972)**. The uncertainties associated with the luminescence and dosimetry data are random; the uncertainties mentioned on the optical ages are the overall uncertainties. The systematic errors taken into account include: 2% beta source calibration, 3% conversion factors, 5% attenuation and etching factors, 3% gamma spectrometer calibration, 15% cosmic radiation, 25% water content. All uncertainties represent 1 $\sigma$ . Specific activities were measured using gamma spectrometry and the ages were determined considering 15% water content; adopted alpha efficiency factor was 0.04 $\pm$ 0.02 for 4-11  $\mu$ m quartz and 0.08 $\pm$ 0.02 for polymineral 4-11  $\mu$ m fine grains, respectively (**Rees-Jones, 1995**). The contribution of cosmic radiation was taken into account and calculated accordingly to **Prescott and Hutton (1994)**. Equivalent doses presented in this table are not corrected for residuals. (\*) represents the pIRIR ages calculated using the modern analogue sample for residual correction.

Sample code	Depth (cm)	Equivalent dose (Gy)			Radionuclide concentration			Annual dose			Age (ka)			Age (ka) (MA) *	
		4-11 $\mu$ m quartz	pIRIR <sub>225</sub> pfg	pIRIR <sub>290</sub> pfg	Ra-226	Th-232	K-40	4-11 $\mu$ m quartz	pIRIR <sub>225</sub> pfg	pIRIR <sub>290</sub> pfg	4-11 $\mu$ m quartz	pIRIR <sub>225</sub> pfg	pIRIR <sub>290</sub> pfg	pIRIR <sub>225</sub> pfg	pIRIR <sub>290</sub> pfg
NZ 6	10	1.3 $\pm$ 0.1	7.5 $\pm$ 0.5	23 $\pm$ 2	42 $\pm$ 2	48 $\pm$ 2	607 $\pm$ 17	4.1 $\pm$ 0.07	4.6 $\pm$ 0.07	4.6 $\pm$ 0.07	0.3 $\pm$ 0.04	1.2 $\pm$ 0.2	4 $\pm$ 0.5		
NZ 7	30	26 $\pm$ 0.3	72 $\pm$ 1	111 $\pm$ 5	50 $\pm$ 2	42 $\pm$ 1	604 $\pm$ 16	4.0 $\pm$ 0.06	4.5 $\pm$ 0.07	4.5 $\pm$ 0.07	6.3 $\pm$ 0.6	15 $\pm$ 1	23 $\pm$ 2	14 $\pm$ 1	20 $\pm$ 2
NZ 8	50	32 $\pm$ 2	72 $\pm$ 1	114 $\pm$ 5	38 $\pm$ 2	30 $\pm$ 1	567 $\pm$ 17	2.9 $\pm$ 0.05	3.7 $\pm$ 0.07	3.7 $\pm$ 0.07	11 $\pm$ 1	19 $\pm$ 2	29 $\pm$ 3	17 $\pm$ 2	24 $\pm$ 2
NZ 9	67	39 $\pm$ 3	63 $\pm$ 1	107 $\pm$ 6	29 $\pm$ 0.2	22 $\pm$ 1	524 $\pm$ 14	2.9 $\pm$ 0.05	3.1 $\pm$ 0.05	3.1 $\pm$ 0.05	13 $\pm$ 2	19 $\pm$ 2	32 $\pm$ 3	18 $\pm$ 2	27 $\pm$ 3
NZ 10	85	43 $\pm$ 1	79 $\pm$ 2	121 $\pm$ 5	47 $\pm$ 3	30 $\pm$ 1	535 $\pm$ 13	3.5 $\pm$ 0.07	3.9 $\pm$ 0.08	3.9 $\pm$ 0.08	12 $\pm$ 1	20 $\pm$ 2	30 $\pm$ 3	19 $\pm$ 2	26 $\pm$ 3
NZ 11	109	46 $\pm$ 1	71 $\pm$ 1	90 $\pm$ 2	41 $\pm$ 1	26 $\pm$ 2	443 $\pm$ 14	3.0 $\pm$ 0.06	3.3 $\pm$ 0.07	3.3 $\pm$ 0.07	16 $\pm$ 1	21 $\pm$ 2	26 $\pm$ 2	19 $\pm$ 2	20 $\pm$ 2
NZ 12	129	41 $\pm$ 2	70 $\pm$ 1	99 $\pm$ 4	34 $\pm$ 1	27 $\pm$ 2	485 $\pm$ 13	3.0 $\pm$ 0.05	3.3 $\pm$ 0.05	3.3 $\pm$ 0.05	14 $\pm$ 1	21 $\pm$ 2	29 $\pm$ 3	19 $\pm$ 2	23 $\pm$ 2

**Table 2.** ESR signal intensities of Al-h, Ti (option A, B, D), “peroxy”, and E' centres, for fractions 4-11, 63-90, 90-125, 125-180, 180-250  $\mu\text{m}$  and calibration quartz.

Sample	Al	st err	Ti A	st err	Ti B	st err	Ti D	st err	peroxy	st err	E'	st err
4-11 $\mu\text{m}$	1.5939	0.0056	0.0769	0.0112	0.0429	0.0080	0.0610	0.0070	2.2026	0.0099	0.4766	0.0073
63-90 $\mu\text{m}$	0.5596	0.0041	0.2141	0.0047	0.0687	0.0067	0.1295	0.0045	0.5018	0.0102	0.1571	0.0062
90-125 $\mu\text{m}$	0.5641	0.0082	0.1778	0.0104	0.0611	0.0072	0.1143	0.0094	0.4660	0.0016	0.1317	0.0020
125-180 $\mu\text{m}$	0.7602	0.0073	0.1557	0.0028	0.0842	0.0065	0.0966	0.0033	0.4569	0.0053	0.1430	0.0008
180-250 $\mu\text{m}$	0.7250	0.0105	0.1304	0.0222	0.0934	0.0005	0.0774	0.0117	0.4598	0.0093	0.0943	0.0030
Calibration quartz	1.7286	0.0158	0.0968	0.0028	0.0598	0.0040	0.0576	0.0024	0.5107	0.0132	0.4435	0.0196





Click here to access/download  
**Supplementary File**  
Supplementary Material.docx



### **Declaration of competing interest**

The authors declare that they have no known competing financial interests or personal relationship that could have appeared to influence the work reported in this paper.